REPORT DOCUMENTATION PAGE

Form Approved OMB NO. 0704-0188

1. REPORT DATE (DD-MM-YYYY)	2. REPORT TYPE	3. DATES COVERED (From - To)
23-06-2008	Final Report	15-Jul-2007 - 14-Apr-2008

4. TITLE AND SUBTITLE
Hopping Rotochute

5a. CONTRACT NUMBER
W911NF-07-1-0487

5b. GRANT NUMBER

5c. PROGRAM ELEMENT NUMBER
611102

6. AUTHORS
Mark Costello, Eric Beyer

5d. PROJECT NUMBER

5e. TASK NUMBER

5f. WORK UNIT NUMBER

7. PERFORMING ORGANIZATION NAMES AND ADDRESSES
Georgia Institute of Technology
Office Of Contract Administration
Program Initiation Division
Atlanta, GA 30332 -0420

8. PERFORMING ORGANIZATION REPORT NUMBER

9. SPONSORING/MONITORING AGENCY NAME(S) AND ADDRESS(ES)
U.S. Army Research Office
P.O. Box 12211
Research Triangle Park, NC 27709-2211

10. SPONSOR/MONITOR'S ACRONYM(S)
ARO

11. SPONSOR/MONITOR'S REPORT NUMBER(S)
53302-CI-II.1

12. DISTRIBUTION AVAILIBILITY STATEMENT
Approved for Public Release; Distribution Unlimited

13. SUPPLEMENTARY NOTES
The views, opinions and/or findings contained in this report are those of the author(s) and should not contrued as an official Department of the Army position, policy or decision, unless so designated by other documentation.

14. ABSTRACT
Future military operations will rely much more heavily on robotic systems to perform a variety of missions. Ultimately, the success of these robots lies in the basic robot configuration being properly tailored to the intended application. A new hybrid micro vehicle configuration, called a hopping rotochute has been created. The hopping rotochute configuration is optimized to operate within small interior spaces. The vehicle is propelled upward by a small rotor that is powered in short bursts so the vehicle hops into the air under power and then falls to the ground when unpowered. The mass properties and exterior shape of the main body of the vehicle are designed to be self-righting so no matter what orientation the vehicle lands it always

15. SUBJECT TERMS
Rotorcraft, micro air vehicle

16. SECURITY CLASSIFICATION OF:			17. LIMITATION OF ABSTRACT	15. NUMBER OF PAGES	19a. NAME OF RESPONSIBLE PERSON
a. REPORT	b. ABSTRACT	c. THIS PAGE			Mark Costello
U	U	U	SAR		19b. TELEPHONE NUMBER 404-385-4303

Report Title

Hopping Rotochute

ABSTRACT

Future military operations will rely much more heavily on robotic systems to perform a variety of missions. Ultimately, the success of these robots lies in the basic robot configuration being properly tailored to the intended application. A new hybrid micro vehicle configuration, called a hopping rotochute has been created. The hopping rotochute configuration is optimized to operate within small interior spaces. The vehicle is propelled upward by a small rotor that is powered in short bursts so the vehicle hops into the air under power and then falls to the ground when unpowered. The mass properties and exterior shape of the main body of the vehicle are designed to be self-righting so no matter what orientation the vehicle lands it always rotates into its nominal position once on the ground. To control the direction of movement of the vehicle, an internal mass is rotated around the perimeter of the body to tilt the main body in the desired direction before a given launch. Performance of this new vehicle has been predicted with a dynamic simulation model with good results. A prototype hopping rotochute has been constructed and flight tested in the Georgia Tech Indoor Flight Facility.

List of papers submitted or published that acknowledge ARO support during this reporting period. List the papers, including journal references, in the following categories:

(a) Papers published in peer-reviewed journals (N/A for none)

Number of Papers published in peer-reviewed journals: 0.00

(b) Papers published in non-peer-reviewed journals or in conference proceedings (N/A for none)

1. M. Costello, E. Beyer, “Performance of a Projectile/Rotor Kinetic Energy Reduction System,” AHS International Specialist Meeting, Unmanned Rotorcraft: Design, Control, and Testing, Chandler, AZ, 2007.

2. E. Beyer, M. Costello, “Performance of a Hopping Rotochute,” European Rotorcraft Forum, Liverpool, England, 2008.

Number of Papers published in non peer-reviewed journals: 2.00

(c) Presentations

Number of Presentations: 0.00

Non Peer-Reviewed Conference Proceeding publications (other than abstracts):

Number of Non Peer-Reviewed Conference Proceeding publications (other than abstracts): 0

Peer-Reviewed Conference Proceeding publications (other than abstracts):

Number of Peer-Reviewed Conference Proceeding publications (other than abstracts): 0

(d) Manuscripts

Number of Manuscripts: 0.00

Number of Inventions:

Graduate Students

NAME	PERCENT_SUPPORTED
Eric Beyer	1.00
FTE Equivalent:	**1.00**
Total Number:	**1**

Names of Post Doctorates

NAME	PERCENT_SUPPORTED
FTE Equivalent:	
Total Number:	

Names of Faculty Supported

NAME	PERCENT_SUPPORTED	National Academy Member
Mark Costello	0.05	No
FTE Equivalent:	**0.05**	
Total Number:	**1**	

Names of Under Graduate students supported

NAME	PERCENT_SUPPORTED
FTE Equivalent:	
Total Number:	

Student Metrics

This section only applies to graduating undergraduates supported by this agreement in this reporting period

The number of undergraduates funded by this agreement who graduated during this period:	0.00
The number of undergraduates funded by this agreement who graduated during this period with a degree in science, mathematics, engineering, or technology fields:.....	0.00
The number of undergraduates funded by your agreement who graduated during this period and will continue to pursue a graduate or Ph.D. degree in science, mathematics, engineering, or technology fields:.....	0.00
Number of graduating undergraduates who achieved a 3.5 GPA to 4.0 (4.0 max scale):	0.00
Number of graduating undergraduates funded by a DoD funded Center of Excellence grant for Education, Research and Engineering:	0.00
The number of undergraduates funded by your agreement who graduated during this period and intend to work for the Department of Defense	0.00
The number of undergraduates funded by your agreement who graduated during this period and will receive scholarships or fellowships for further studies in science, mathematics, engineering or technology fields:	0.00

Names of Personnel receiving masters degrees

NAME
Total Number:

Names of personnel receiving PHDs

NAME
Eric Beyer
Total Number: 1

Names of other research staff

NAME	PERCENT_SUPPORTED
FTE Equivalent:	
Total Number:	

Sub Contractors (DD882)

Inventions (DD882)

Performance of a Hopping Rotochute

Eric Beyer[*] and Mark Costello[1]

School of Aerospace Engineering

Georgia Institute of Technology

Atlanta, Georgia 30332

Nomenclature

$\vec{a}_{B/I}, \vec{a}_{H/I}, \vec{a}_{T/I}$: Acceleration of base, rotor, and system mass center with respect to the inertial frame

C_D, C_L, C_M : Aerodynamic drag, lift, and moment coefficients

c : Coefficient of damping

$\overline{c}$: Aerodynamic reference chord

c_M : Viscous damping coefficient

$\vec{F}_C$: Contact force applied to base in base body reference frame

$\vec{F}_{CST}$: Constraint force in base body reference frame

$\vec{F}_A^B, \vec{F}_A^H$: Aerodynamic force of base and rotor in base body reference frame

$\vec{F}_W^B, \vec{F}_W^H$: Weight of base and rotor in base body reference frame

g : Acceleration of gravity

$\vec{H}_{B/I}^B$: Angular momentum of base with respect to inertial frame about base mass center

$\vec{H}_{H/I}^H$: Angular momentum of rotor with respect to inertial frame about rotor mass center

I : Effective inertia matrix in base body reference frame

$I_{XX}^B, I_{YY}^B, I_{ZZ}^B, I_{XY}^B, I_{XZ}^B, I_{YZ}^B$: Base inertia matrix terms about base mass center in base body reference frame.

---

[*] Graduate Research Assistant, Member AIAA.

[1] Sikorsky Associate Professor, Associate Fellow AIAA.

$I_{XX}^{H}, I_{YY}^{H}, I_{ZZ}^{H}, I_{XY}^{H}, I_{XZ}^{H}, I_{YZ}^{H}$: Rotor inertia matrix terms about rotor mass center in base body reference frame.

k : Spring constant

L_T, M_T, N_T : Total applied moment components about connection point in base body reference frame

m_B, m_H, m_T : Mass of base, rotor, and system

$\vec{M}_C$: Contact moment applied to base about connection point in base body reference frame

$\vec{M}_{CST}$: Constraint moment in base body reference frame

$\vec{M}_G^B, \vec{M}_G^H$: Total external moment applied to base and rotor about connection point in base body reference frame

$\vec{M}_M$: Motor moment in base body reference frame

p, q, r : Components of angular velocity vector of base in base body reference frame

r_H : Angular velocity of rotor along yaw axis in base body reference frame

$\vec{r}_{D\to F}$: Position vector from some point D to some point F

S : Aerodynamic reference area

$\vec{s}$: Spring deflection distance vector

T_{BH} : Transformation matrix from the rotor to the base body reference frame

T_{HR} : Transformation matrix from the rotor blade to the rotor body reference frame

u, v, w : Components of velocity vector of system mass center in base body reference frame

u_A, v_A, w_A : Relative aerodynamic velocity components

w_F, w_{UF} : Filtered and unfiltered inflow velocity

x_I, y_I, z_I : Components of position vector of system mass center in an inertial reference frame

X_T, Y_T, Z_T : Total applied force components in base body reference frame

ρ : Air density

ϕ, θ, ψ : Euler roll, pitch, and yaw angles of base

$\phi_R, \gamma_R, \theta_R$: Rotor blade azimuthal, coning, and pitch angle

γ : Euler yaw angle of the hub

μ : Coefficient of friction

τ : Inflow time constant

$\vec{\omega}_{B/I}, \vec{\omega}_{H/I}$: Angular velocity of base and rotor with respect to the inertial frame

$\vec{\omega}_{B/H}$: Angular velocity of rotor with respect to the base body reference frame

I. Introduction

Future military operations will rely much more heavily on robotic systems to perform a variety of missions. Ultimately, the success of these robots lies in the basic robot configuration being properly tailored to the intended application. For complicated battlefield missions, vehicle/sensor suite/control laws specialized and matched to the intended missions is critical to the performance of the overall system. One such difficult mission is exploring the interior spaces of caves and damaged buildings. Current micro ground and air vehicle configurations both have significant limitations to perform this mission well. A new hybrid micro vehicle configuration, called a hopping rotochute, is investigated here. The hopping rotochute configuration, shown in Fig. 1, is optimized to operate within small interior spaces. The vehicle is propelled upward by a motor-driven rotor that is powered in short bursts so the vehicle hops into the air under power and then descends to the ground when unpowered. The mass properties and exterior shape of the main body (base) of the vehicle are designed to be self-righting so no matter what orientation the vehicle lands, it always rotates into its nominal position once on the ground. To control the direction of movement of the vehicle, an internal mass is rotated around the perimeter of the body to tilt the main body in the desired direction before a given launch. This paper investigates the potential of this new hybrid micro vehicle, including a dynamic model and system simulation results.

II. Dynamic Model

A schematic of the hopping rotochute with associated reference frames and points is given in Fig. 2. The mathematical model of this system includes three translational and four rotational rigid body degrees of freedom. The translational degrees of freedom are the three position components of the system mass center. The rotational

degrees of freedom are the Euler yaw, pitch, and roll angles of the body as well as the rotor yaw angle. The translational and rotational kinematic equations of motion of the hopping rotochute are given in Eqs. (1) and (2)[1,2].

$$\begin{Bmatrix} \dot{x}_I \\ \dot{y}_I \\ \dot{z}_I \end{Bmatrix} = \begin{bmatrix} c_\theta c_\psi & s_\phi s_\theta c_\psi - c_\phi s_\psi & c_\phi s_\theta c_\psi + s_\phi s_\psi \\ c_\theta s_\psi & s_\phi s_\theta s_\psi + c_\phi c_\psi & c_\phi s_\theta s_\psi - s_\phi c_\psi \\ -s_\theta & s_\phi c_\theta & c_\phi c_\theta \end{bmatrix} \begin{Bmatrix} u \\ v \\ w \end{Bmatrix} \tag{1}$$

$$\begin{Bmatrix} \dot{\phi} \\ \dot{\theta} \\ \dot{\psi} \\ \dot{\gamma} \end{Bmatrix} = \begin{bmatrix} 1 & s_\phi t_\theta & c_\phi t_\theta & 0 \\ 0 & c_\phi & -s_\phi & 0 \\ 0 & s_\phi / c_\theta & c_\phi / c_\theta & 0 \\ 0 & 0 & 0 & 1 \end{bmatrix} \begin{Bmatrix} p \\ q \\ r \\ r_H \end{Bmatrix} \tag{2}$$

The standard shorthand is used for trigonometric functions where $\cos(\alpha) \equiv c_\alpha$, $\sin(\alpha) \equiv s_\alpha$, and $\tan(\alpha) \equiv t_\alpha$. The translational kinetic equations of motion are derived by splitting the two body system at the bearing connection point and summing the forces about the respective mass centers as shown in Eq. (3) and (4).

$$m_B \vec{a}_{B/I} = \vec{F}_W^B + \vec{F}_A^B + \vec{F}_C + \vec{F}_{CST} \tag{3}$$

$$m_H \vec{a}_{H/I} = \vec{F}_W^H + \vec{F}_A^H - \vec{F}_{CST} \tag{4}$$

By adding Eqs. (3) and (4) together, the constraint force $(\vec{F}_{CST})$ is eliminated, while $m_B \vec{a}_{B/I} + m_H \vec{a}_{H/I}$ is the definition of the system mass center. The resulting translational dynamic equations of motion of the system are given in Eq. (5).

$$m_T \vec{a}_{T/I} = \vec{F}_W^B + \vec{F}_W^H + \vec{F}_A^B + \vec{F}_A^H + \vec{F}_C \tag{5}$$

Expressing Eq. (5) in the base body frame results in the translational kinetic equations of motion of the hopping rotochute shown in Eq. (6)

$$\begin{Bmatrix} \dot{u} \\ \dot{v} \\ \dot{w} \end{Bmatrix} = \begin{Bmatrix} X_T / m_T \\ Y_T / m_T \\ Z_T / m_T \end{Bmatrix} - \begin{bmatrix} 0 & -r & q \\ r & 0 & -p \\ -q & p & 0 \end{bmatrix} \begin{Bmatrix} u \\ v \\ w \end{Bmatrix} \tag{6}$$

where X_T, Y_T, and Z_T are the components of the total force expressed in the base body reference frame.

The rotational kinetic equations of motion are derived in a similar manner by splitting the system into two bodies at the connection point and summing the external moments about this connection point as shown in Eqs. (7) and (8).

$$\frac{{}^{I}d\vec{H}^{B}_{B/I}}{dt} + \vec{r}_{G\to B} \times m_B \vec{a}_{B/I} = \vec{M}^{B}_{G} \tag{7}$$

$$\frac{{}^{I}d\vec{H}^{H}_{H/I}}{dt} + \vec{r}_{G\to H} \times m_H \vec{a}_{H/I} = \vec{M}^{H}_{G} \tag{8}$$

The moments on the right hand side of Eqs. (7) and (8) contain contributions from many sources as shown in Eqs. (9) and (10),

$$\vec{M}^{B}_{G} = \vec{r}_{G\to B} \times \vec{F}^{B}_{W} + \vec{M}^{B}_{A} + \vec{M}_{M} + \vec{M}_{C} + \vec{M}_{CST} \tag{9}$$

$$\vec{M}^{H}_{G} = \vec{r}_{G\to H} \times \vec{F}^{H}_{W} + \vec{M}^{H}_{A} - \vec{M}_{M} - \vec{M}_{CST} \tag{10}$$

In order to avoid the calculation of the constraint moment $(\vec{M}_{CST})$, Eqs. (9) and (10) are dotted with $\vec{K}_B$ since the bodies are not constrained along this direction. This results in two rotational kinetic equations of motion. The other two rotational dynamic differential equations are obtained by adding Eqs. (9) and (10) and dotting the resulting equation with $\vec{I}_B$ and $\vec{J}_B$. These four equations can be assembled to represent the entire set of rotational dynamics as shown in Eq. (11).

$$\begin{bmatrix} I_{1,1} & I_{1,2} & I_{1,3} & I_{1,4} \\ I_{2,1} & I_{2,2} & I_{2,3} & I_{2,4} \\ I_{3,1} & I_{3,2} & I_{3,3} & I_{3,4} \\ I_{4,1} & I_{4,2} & I_{4,3} & I_{4,4} \end{bmatrix} \begin{Bmatrix} \dot{p} \\ \dot{q} \\ \dot{r} \\ \dot{r}_H \end{Bmatrix} = \begin{Bmatrix} B_1 \\ B_2 \\ B_3 \\ B_4 \end{Bmatrix} \tag{11}$$

The terms in the effective inertia matrix are given by Eqs. (12) through (27) where the components of the position vectors expressed in the base body frame are represented by SL, BL, and WL along $\vec{I}_B$, $\vec{J}_B$, $\vec{K}_B$ respectively.

$$I_{1,1} = I^{B}_{XZ} - m_B \left(SL_{G\to B} WL_{T\to B} \right) \tag{12}$$

$$I_{1,2} = I^{B}_{YZ} - m_B \left(BL_{G\to B} WL_{T\to B} \right) \tag{13}$$

$$I_{1,3} = I^{B}_{ZZ} + m_B \left(BL_{G\to B} BL_{T\to B} + SL_{G\to B} SL_{T\to B} \right) \tag{14}$$

$$I_{1,4} = 0 \tag{15}$$

$$I_{2,1} = I^{H}_{XZ} - m_H \left(SL_{G\to H} WL_{G\to H} + SL_{G\to H} WL_{T\to G} \right) \tag{16}$$

$$I_{2,2} = I^{H}_{YZ} - m_H \left(BL_{G\to H} WL_{G\to H} + BL_{G\to H} WL_{T\to G} \right) \tag{17}$$

$$I_{2,3} = I_{ZZ}^{H} + m_H \left(BL_{G\to H} BL_{G\to H} + SL_{G\to H} SL_{G\to H} + BL_{G\to H} BL_{T\to G} + SL_{G\to H} SL_{T\to G} \right) \tag{18}$$

$$I_{2,4} = I_{ZZ}^{H} + m_H \left(BL_{G\to H} BL_{G\to H} + SL_{G\to H} SL_{G\to H} \right) \tag{19}$$

$$\begin{aligned} I_{3,1} = {} & I_{XX}^{B} + I_{XX}^{H} + m_B \left(WL_{G\to B} WL_{T\to B} + BL_{G\to B} BL_{T\to B} \right) + \\ & m_H \left(WL_{G\to H} WL_{G\to H} + BL_{G\to H} BL_{G\to H} + WL_{G\to H} WL_{T\to G} + BL_{G\to H} BL_{T\to G} \right) \end{aligned} \tag{20}$$

$$I_{3,2} = I_{XY}^{B} + I_{XY}^{H} - m_B \left(BL_{G\to B} SL_{T\to B} \right) - m_H \left(BL_{G\to H} SL_{G\to H} + BL_{G\to H} SL_{T\to G} \right) \tag{21}$$

$$I_{3,3} = I_{XZ}^{B} + I_{XZ}^{H} - m_B \left(WL_{G\to B} SL_{T\to B} \right) - m_H \left(WL_{G\to H} SL_{G\to H} + WL_{G\to H} SL_{T\to G} \right) \tag{22}$$

$$I_{3,4} = I_{XZ}^{H} - m_H \left(WL_{G\to H} SL_{G\to H} \right) \tag{23}$$

$$I_{4,1} = I_{XY}^{B} + I_{XY}^{H} - m_B \left(SL_{G\to B} BL_{T\to B} \right) - m_H \left(SL_{G\to H} BL_{G\to H} + SL_{G\to H} BL_{T\to G} \right) \tag{24}$$

$$\begin{aligned} I_{4,2} = {} & I_{YY}^{B} + I_{YY}^{H} + m_B \left(WL_{G\to B} WL_{T\to B} + SL_{G\to B} SL_{T\to B} \right) + \\ & m_H \left(WL_{G\to H} WL_{G\to H} + SL_{G\to H} SL_{G\to H} + WL_{G\to H} WL_{T\to G} + SL_{G\to H} SL_{T\to G} \right) \end{aligned} \tag{25}$$

$$I_{4,3} = I_{YZ}^{B} + I_{YZ}^{H} - m_B \left(WL_{G\to B} BL_{T\to B} \right) - m_H \left(WL_{G\to H} BL_{G\to H} + WL_{G\to H} BL_{T\to G} \right) \tag{26}$$

$$I_{4,4} = I_{YZ}^{H} - m_H \left(WL_{G\to H} BL_{G\to H} \right) \tag{27}$$

The right hand side of Eq. (11) is given by Eqs. (28) through (31).

$$B_1 = \left[\vec{M}_G^{B} - \vec{\omega}_{B/I} \times \left(I^{B} \vec{\omega}_{B/I} \right) - m_B \vec{r}_{G\to B} \times \left(\vec{a}_{T/I} + \vec{\omega}_{B/I} \times \left(\vec{\omega}_{B/I} \times \vec{r}_{T\to B} \right) \right) \right] \cdot \vec{K}_B \tag{28}$$

$$B_2 = \begin{bmatrix} \vec{M}_G^{H} - I^{H} \left(\vec{\omega}_{B/H} \times \vec{\omega}_{H/I} \right) - \vec{\omega}_{H/I} \times \left(I^{H} \vec{\omega}_{H/I} \right) - \\ m_B \vec{r}_{G\to H} \times \left(\vec{a}_{T/I} + \vec{\omega}_{B/I} \times \left(\vec{\omega}_{B/I} \times \vec{r}_{T\to G} \right) + \left(\vec{\omega}_{B/I} \times \vec{\omega}_{H/I} \right) \times \vec{r}_{G\to H} + \vec{\omega}_{H/I} \times \left(\vec{\omega}_{H/I} \times \vec{r}_{G\to H} \right) \right) \end{bmatrix} \cdot \vec{K}_B \tag{29}$$

$$B_3 = \begin{bmatrix} \vec{M}_G^{B} - \vec{\omega}_{B/I} \times \left(I^{B} \vec{\omega}_{B/I} \right) - m_B \vec{r}_{G\to B} \times \left(\vec{a}_{T/I} + \vec{\omega}_{B/I} \times \left(\vec{\omega}_{B/I} \times \vec{r}_{T\to B} \right) \right) + \\ \vec{M}_G^{H} - I^{H} \left(\vec{\omega}_{B/H} \times \vec{\omega}_{H/I} \right) - \vec{\omega}_{H/I} \times \left(I^{H} \vec{\omega}_{H/I} \right) - \\ m_B \vec{r}_{G\to H} \times \left(\vec{a}_{T/I} + \vec{\omega}_{B/I} \times \left(\vec{\omega}_{B/I} \times \vec{r}_{T\to G} \right) + \left(\vec{\omega}_{B/I} \times \vec{\omega}_{H/I} \right) \times \vec{r}_{G\to H} + \vec{\omega}_{H/I} \times \left(\vec{\omega}_{H/I} \times \vec{r}_{G\to H} \right) \right) \end{bmatrix} \cdot \vec{I}_B \tag{30}$$

$$B_4 = \begin{bmatrix} \vec{M}_G^{B} - \vec{\omega}_{B/I} \times \left(I^{B} \vec{\omega}_{B/I} \right) - m_B \vec{r}_{G\to B} \times \left(\vec{a}_{T/I} + \vec{\omega}_{B/I} \times \left(\vec{\omega}_{B/I} \times \vec{r}_{T\to B} \right) \right) + \\ \vec{M}_G^{H} - I^{H} \left(\vec{\omega}_{B/H} \times \vec{\omega}_{H/I} \right) - \vec{\omega}_{H/I} \times \left(I^{H} \vec{\omega}_{H/I} \right) - \\ m_B \vec{r}_{G\to H} \times \left(\vec{a}_{T/I} + \vec{\omega}_{B/I} \times \left(\vec{\omega}_{B/I} \times \vec{r}_{T\to G} \right) + \left(\vec{\omega}_{B/I} \times \vec{\omega}_{H/I} \right) \times \vec{r}_{G\to H} + \vec{\omega}_{H/I} \times \left(\vec{\omega}_{H/I} \times \vec{r}_{G\to H} \right) \right) \end{bmatrix} \cdot \vec{J}_B \tag{31}$$

The resulting rotational dynamic equations of motion of the hopping rotochute expressed in the base body frame are given in Eq. (32).

$$\begin{Bmatrix} \dot{p} \\ \dot{q} \\ \dot{r} \\ \dot{r}_H \end{Bmatrix} = \left[I \right]^{-1} \begin{Bmatrix} B_1 \\ B_2 \\ B_3 \\ B_4 \end{Bmatrix} \tag{32}$$

Forces and Moments

The weight of the base and rotor expressed in the base body frame are given in Eqs. (33) and (34) respectively.

$$\vec{F}_W^{\,B} = \begin{Bmatrix} X_W^B \\ Y_W^B \\ Z_W^B \end{Bmatrix} = m_B g \begin{Bmatrix} -s_\theta \\ s_\phi c_\theta \\ c_\phi c_\theta \end{Bmatrix} \tag{33}$$

$$\vec{F}_W^{\,H} = \begin{Bmatrix} X_W^H \\ Y_W^H \\ Z_W^H \end{Bmatrix} = m_H g \begin{Bmatrix} -s_\theta \\ s_\phi c_\theta \\ c_\phi c_\theta \end{Bmatrix} \tag{34}$$

The aerodynamic force from the base is calculated assuming that only drag acts on this body as shown in Eq. (35).

$$\vec{F}_A^{\,B} = \begin{Bmatrix} X_A^B \\ Y_A^B \\ Z_A^B \end{Bmatrix} = -\frac{1}{2} \rho \sqrt{u_{A_B}^2 + v_{A_B}^2 + w_{A_B}^2}\, S_B C_{D_B} \begin{Bmatrix} u_{A_B} \\ v_{A_B} \\ w_{A_B} \end{Bmatrix} \tag{35}$$

The aerodynamic moment due to the base body about the connection point is calculated using

$$\vec{M}_A^{\,B} = \begin{Bmatrix} L_A^B \\ M_A^B \\ N_A^B \end{Bmatrix} = \begin{bmatrix} 0 & -WL_{G\to CP_B} & BL_{G\to CP_B} \\ WL_{G\to CP_B} & 0 & -SL_{G\to CP_B} \\ -BL_{G\to CP_B} & SL_{G\to CP_B} & 0 \end{bmatrix} \begin{Bmatrix} X_A^B \\ Y_A^B \\ Z_A^B \end{Bmatrix} \tag{36}$$

The total aerodynamic force due to the rotor is calculated by summing the forces from each individual (i^{th}) rotor blade as shown in Eq. (37).

$$\begin{Bmatrix} X_A^H \\ Y_A^H \\ Z_A^H \end{Bmatrix} = \sum_{i=1}^{NR} \left(\begin{Bmatrix} X_{Ri} \\ Y_{Ri} \\ Z_{Ri} \end{Bmatrix} \right) \tag{37}$$

where *NR* represents the number of rotor blades. The aerodynamic force due to i^{th} rotor blade is calculated by summing the forces from each j^{th} blade element[3] of the rotor blade and is given by

$$\begin{Bmatrix} X_{Ri} \\ Y_{Ri} \\ Z_{Ri} \end{Bmatrix} = \sum_{j=1}^{NE} \left(\begin{Bmatrix} X_{Ej} \\ Y_{Ej} \\ Z_{Ej} \end{Bmatrix} \right) \tag{38}$$

$$\begin{Bmatrix} X_{E_j} \\ Y_{E_j} \\ Z_{E_j} \end{Bmatrix} = \left[T_{BH}\right]\left[T_{HR_j}\right] q_j S_j \begin{Bmatrix} 0 \\ -C_{L_j} c_{\alpha_j} - C_{D_j} s_{\alpha_j} \\ C_{L_j} s_{\alpha_j} - C_{D_j} c_{\alpha_j} \end{Bmatrix} \tag{39}$$

$$q_j = \frac{1}{2}\rho\left(v_{A_j}^2 + w_{A_j}^2\right) \tag{40}$$

$$\alpha_j = \tan^{-1}\left(\frac{v_{A_j}}{w_{A_j}}\right) \tag{41}$$

where *NE* is the number of blade elements on each rotor blade. The transformation matrix from the rotor body frame to the base body frame is given in Eq. (42) and the transformation matrix from the j^{th} blade element to the rotor body frame given in Eq. (43).

$$\left[T_{BH}\right] = \begin{bmatrix} c_\gamma & -s_\gamma & 0 \\ s_\gamma & c_\gamma & 0 \\ 0 & 0 & 1 \end{bmatrix} \tag{42}$$

$$\left[T_{HR_j}\right] = \begin{bmatrix} c_{\phi_{Ri}} c_{\gamma_{Ri}} & c_{\phi_{Ri}} s_{\gamma_{Ri}} s_{\theta_{Ej}} - s_{\phi_{Ri}} c_{\theta_{Rj}} & c_{\phi_{Ri}} s_{\gamma_{Ri}} c_{\theta_{Ej}} + s_{\phi_{Ri}} s_{\theta_{Ej}} \\ s_{\phi_{Ri}} c_{\gamma_{Ri}} & s_{\phi_{Ri}} s_{\gamma_{Ri}} s_{\theta_{Ej}} + c_{\phi_{Ri}} c_{\theta_{Ej}} & s_{\phi_{Ri}} s_{\gamma_{Ri}} c_{\theta_{Ej}} - c_{\phi_{Ri}} s_{\theta_{Ej}} \\ -s_{\gamma_{Ri}} & c_{\gamma_{Ri}} s_{\theta_{Ej}} & c_{\gamma_{Ri}} c_{\theta_{Ej}} \end{bmatrix} \tag{43}$$

As described, each rotor blade is oriented on the rotor with three successive rotations. Starting with the rotor blade body reference frame aligned with the rotor body reference frame, the rotor blade is rotated about the $\vec{K}_H$ axis by the azimuthal angle (ϕ_R), then about the resulting intermediate $\vec{J}$ axis by the coning angle (γ_R), and finally by the pitch angle (θ_R) about the resulting $\vec{I}$ axis. Note that in addition to the rotor blade pitch angle, each rotor

blade can also be twisted. By defining a twist per rotor blade length $\left(\theta_{TWIST}\right)$, the pitch of the blade element is given as

$$\theta_{Ej} = \theta_{Ri} + \theta_{TWIST}\left(SL_{E\to CP_j}\right) \tag{44}$$

The total aerodynamic moment of the rotor about the connection point is calculated in a similar manner by summing the moments from each individual rotor blade as shown in Eq. (45).

$$\vec{M}_A^H = \begin{Bmatrix} L_A^H \\ M_A^H \\ N_A^H \end{Bmatrix} = \sum_{i=1}^{NR}\left(\begin{Bmatrix} L_{Ri} \\ M_{Ri} \\ N_{Ri} \end{Bmatrix}\right) \tag{45}$$

$$\begin{Bmatrix} L_{Ri} \\ M_{Ri} \\ N_{Ri} \end{Bmatrix} = \sum_{j=1}^{NE}\left(\begin{Bmatrix} L_{Ej} \\ M_{Ej} \\ N_{Ej} \end{Bmatrix} + \begin{bmatrix} 0 & -WL_{G\to CP_j} & BL_{G\to CP_j} \\ WL_{G\to CP_j} & 0 & -SL_{G\to CP_j} \\ -BL_{G\to CP_j} & SL_{G\to CP_j} & 0 \end{bmatrix}\begin{Bmatrix} X_{Ej} \\ Y_{Ej} \\ Z_{Ej} \end{Bmatrix}\right) \tag{46}$$

$$\begin{Bmatrix} L_{E_j} \\ M_{E_j} \\ N_{E_j} \end{Bmatrix} = \left[T_{BH}\right]\left[T_{HR_j}\right] q_j S_j \bar{c}_j \begin{Bmatrix} -C_{M_j} \\ 0 \\ 0 \end{Bmatrix} \tag{47}$$

The inflow velocity through the spinning rotor is assumed to be uniform with dynamics described by Eq. (48)

$$\tau \dot{w}_F + w_F = w_{UF} \tag{48}$$

where τ is the time constant associated with the dynamics of the inflow[4]. The unfiltered induced is calculated using both theoretical and empirical curves which account for the different flow states of the induced velocity[5].

The contact forces and moments that act on the base during impact with the ground are calculated based on a soft contact model originally developed by Goyal, Pinson, and Sinden[6,7]. The model uses vertices located around the perimeter of the base body to calculate the contact forces between the base and the ground (assumed to be flat). The contact force associated with each contact point has two components: a normal component $\left(\vec{F}_n\right)$ along the ground normal and a frictional component $\left(\vec{F}_t\right)$ in the tangential plane of contact. Each vertice has a normal and tangential spring attached to it along with a normal and tangential damper. The spring constants along the normal and

tangential directions are defined as k_{1n} and k_{1t} respectively while the damper constants are defined as c_{1n} and c_{1t}. The ground also has similar springs and dampers in these two directions with constants k_{2n}, k_{2t}, c_{2n}, and c_{2t}. Assuming all dampers are non-zero, the force in the normal and tangential directions associated with a given vertice v is,

$$\vec{F}_{n_v} = -\vec{b}_{n_v} \qquad \vec{F}_{t_v} = -\vec{b}_{t_v} + c^* \Delta\vec{w}_{t_v} \tag{49}$$

where

$$c^* = \frac{c_{1t} c_{2t}}{c_{1t} + c_{2t}} \tag{50}$$

$$\vec{b}_{n_v} = \frac{1}{c_{1n} + c_{2n}} \left(c_{2n} k_{1n} \vec{s}_{1n_v} - c_{1n} k_{2n} \vec{s}_{2n_v} + c_{1n} c_{2n} \Delta\vec{u}_{n_v} \right) \tag{51}$$

$$\vec{b}_{t_v} = \frac{1}{c_{1t} + c_{2t}} \left(c_{2t} k_{1t} \vec{s}_{1t_v} - c_{1t} k_{2t} \vec{s}_{2t_v} + c_{1t} c_{2t} \Delta\vec{u}_{t_v} \right) \tag{52}$$

The difference in the absolute velocity of vertice v and the ground along the normal direction and tangential direction is given as $\Delta\vec{u}_{1n_v}$ and $\Delta\vec{u}_{1t_v}$ respectively. The states $\vec{s}_{1n_v}$ and $\vec{s}_{2n_v}$ track the lengths of the normal springs k_{1n} and k_{2n}, while $\vec{s}_{1t_v}$ and $\vec{s}_{2t_v}$ track the lengths of the tangential springs k_{1t} and k_{2t} of each contact point. The tangential force of vertice v is calculated based on the relation given in Eq. (53)

$$\frac{\left|\vec{b}_{t_v}\right|}{\left(1 + \lambda c^*\right)} \le \mu \left|\vec{b}_{n_v}\right| \tag{53}$$

If the relation $\left|\vec{b}_{t_v}\right| \le \mu \left|\vec{b}_{n_v}\right|$ holds true, then a state of stick exits and the variables are calculated as

$$\lambda_v = 0 \qquad \Delta w_{t_v} = 0 \qquad \vec{F}_{t_v} = -\vec{b}_{t_v} \tag{54}$$

If, on the other hand $\left|\vec{b}_{t_v}\right| > \mu \left|\vec{b}_{n_v}\right|$, the variables are calculated using the following equations

$$\lambda_v = \frac{\left|\vec{b}_{t_v}\right| - \mu \left|\vec{b}_{n_v}\right|}{c^* \mu \left|\vec{b}_{n_v}\right|} \qquad \Delta\vec{w}_{t_v} = \frac{\lambda \vec{b}_{t_v}}{\left(1 + \lambda c^*\right)} \qquad \vec{F}_{t_v} = \frac{-\vec{b}_{t_v}}{\left(1 + \lambda c^*\right)} \tag{55}$$

Hence, the contact force and moment applied to the base body in the base body frame about the connection point is given as

$$\vec{F}_C = \left[T_{BI}\right]\sum_{v=1}^{NV}\left(\begin{Bmatrix} F_{nx_v} \\ F_{ny_v} \\ F_{nz_v} \end{Bmatrix} + \begin{Bmatrix} F_{tx_v} \\ F_{ty_v} \\ F_{tz_v} \end{Bmatrix}\right) \tag{56}$$

$$\vec{M}_C = \left[T_{BI}\right]\sum_{v=1}^{NV}\left(\begin{bmatrix} 0 & -WL_{G\to V_v} & BL_{G\to V_v} \\ WL_{G\to V_v} & 0 & -SL_{G\to V_v} \\ -BL_{G\to V_v} & SL_{G\to V_v} & 0 \end{bmatrix}\left(\begin{Bmatrix} F_{nx_v} \\ F_{ny_v} \\ F_{nz_v} \end{Bmatrix} + \begin{Bmatrix} F_{tx_v} \\ F_{ty_v} \\ F_{tz_v} \end{Bmatrix}\right)\right) \tag{57}$$

where *NV* are the number of vertices. The state of the springs associated with each vertice in the contact model is tracked with the following differential equations,

$$\dot{\vec{s}}_{1n_v} = \frac{c_{2n}}{c_{1n}+c_{2n}}\Delta\vec{u}_{n_v} - \frac{1}{c_{1n}+c_{2n}}\left(k_{1n}\vec{s}_{1n_v} + k_{2n}\vec{s}_{2n_v}\right) \tag{58}$$

$$\dot{\vec{s}}_{1t_v} = \frac{c_{2t}}{c_{1t}+c_{2t}}\left(\Delta\vec{u}_{t_v} - \Delta\vec{w}_{t_v}\right) - \frac{1}{c_{1t}+c_{2t}}\left(k_{1t}\vec{s}_{1t_v} + k_{2t}\vec{s}_{2t_v}\right) \tag{59}$$

$$\dot{\vec{s}}_{2n_v} = \frac{-c_{1n}}{c_{1n}+c_{2n}}\Delta\vec{u}_{n_v} - \frac{1}{c_{1n}+c_{2n}}\left(k_{1n}\vec{s}_{1n_v} + k_{2n}\vec{s}_{2n_v}\right) \tag{60}$$

$$\dot{\vec{s}}_{2t_v} = \frac{-c_{1t}}{c_{1t}+c_{2t}}\left(\Delta\vec{u}_{t_v} - \Delta\vec{w}_{t_v}\right) - \frac{1}{c_{1t}+c_{2t}}\left(k_{1t}\vec{s}_{1t_v} + k_{2t}\vec{s}_{2t_v}\right) \tag{61}$$

The motor moment acts only along the $\vec{K}_B$ direction and is given by Eq. (62)

$$\vec{M}_M = \begin{Bmatrix} 0 \\ 0 \\ N_M \end{Bmatrix} \tag{62}$$

During the power on phase, the value of N_M is set to a value representative of a torque produced by a small electric motor. When the power is cycled off, the motor moment can be set to zero in order to represent a frictionless bearing or Eq. (63) can be used to model viscous damping[8].

$$N_M = c_M\left(r_H\right) \tag{63}$$

III. Simulation Results

To investigate the dynamics and performance of a hopping rotochute micro vehicle, the equations of motion described in the preceding section are numerically integrated forward in time using a fourth-order Runge-Kutta algorithm. The hopping rotochute used in this study has a height of 12.7 cm, a base diameter of 10.16 cm, and a rotor radius of 10.16 cm as described in Table 1. The base has a weight of 0.4966 N and has a mass center which is offset from the axis of rotation of the connection point. The rotor weighs 0.052 N (see Table 2) and consists of 3 similar rotor blades arranged symmetrically about the connection point with a chord of 1.9 cm, a coning angle of 0 deg, and a pitch twist of 5 deg. To approximate the shape of the base for the contact analysis, 144 vertices were used in 15 deg increments around the perimeter of the base at 6 different base heights. The spring and damper coefficients of the base and the ground were assumed to be the same with a spring constant of 50,000 N/m and a damper constant of 400 N-s/m, while the coefficient of friction between the base and the ground is 1.6. The initial conditions used in this study are outlined in Table 3 and represent the hopping rotochute resting on the ground without any motion.

An example time simulation using the mass properties and initial condition stated above was ran and the resulting time histories are given in Fig. 3 through 8. As shown, the hopping rotochute performs two hops. The hops are initiated when the base of the hopping rotochute reaches equilibrium. Once the base is stationary, the rotor is spun up using a motor moment of 0.3 N-m for a duration of 0.5 sec. After the powered climb has terminated, the rotor is free to spin about the bearing connection point. As shown in Fig. 3 and 5, the hopping rotochute is powered at times of 0.17 and 4.5 sec, reaching altitudes of 5.2 and 4.9 m respectively. Figure 4 shows that the system travels approximately 2.6 m during the first hop and 3.7 m during the second. The difference in the altitude and cross range for the two hops is attributed to the system being oriented differently when the hop is initiated. Figure 6 presents the time history of the pitch angle of the system versus time. As shown, during the power off descent the hopping rotochute tends to cone. The landing after the first hop results in little pitch change, whereas the second landing involves major pitch changes. This is attributed to the increased coning motion of the hopping rotochute during the second descent. Note that the low center of gravity allows the system to upright itself after each impact. As shown in Figure 7, the hopping rotochute reaches a maximum absolute vertical velocity of 7.4 m/s during powered flight and impacts the ground with a vertical velocity of 5.2 m/s. Figure 8 demonstrates that the base body yaw rate

remains rather small except during impact when the value increases momentarily. As shown in Fig. 9, the motor moment spins the rotor up to angular speeds of -1480 rad/s and the aerodynamic moments tend to slow the rotor once the motor moment is cycled off.

The figures presented demonstrate the hopping rotochutes ability to navigate in small spaces while always up righting itself upon impact. The next step, which will be included in the final report, will address the performance of these hybrid micro vehicles. Trade studies will be performed which will provide insight on the maximum range and endurance of these systems with and without ceiling limits for given battery capacities.

IV. Prototype Hardware

An example hopping rotochute has been constructed and flight tested. The prototype is shown in Figure 9. The prototype was flight tested in the Georgia Tech Indoor Flight Facility to demonstrate its flight capability shown in Figure 10. The flight tests demonstrated the basic hopping capability of the rotorchute and its ability to be actively controlled. Figures 11 and 12 show an example hopping sequence.

References

[1]Etkin, B., *Dynamics of Atmospheric Flight*, Wiley, New York, 1972.

[2]Costello, M., Peterson, A., "Linear Theory of a Dual-Spin Projectile in Atmospheric Flight, *Journal of Guidance, Control, and Dynamics*, Vol. 23, No. 5, September-October 2000.

[3]Johnson, W., *Helicopter Theory*, Princeton, New Jersey, 1980.

[4]Pitt, D., Peters, D., "Theoretical Prediction of Dynamic-Inflow Derivatives," *Vertica*, Vol. 5, pp. 21-34, 1980.

[5]Gessow, A., Myers, G., *Aerodynamics of the Helicopter*, College Parks Press, U.S., 1985.

[6]Goyal, S., Pinson, E. N., Sinden, F. W., "Simulation of Dynamics of Interacting Rigid Bodies Including Friction I: General Problem and Contact Model," *Engineering with Computers*, Vol. 10, pp. 162-174, 1994.

[7]Goyal, S., Pinson, E. N., Sinden, F. W., "Simulation of Dynamics of Interacting Rigid Bodies Including Friction II: Software System Design and Implementation," *Engineering with Computers*, Vol. 10, pp. 175-195, 1994.

[8]Close, C. M., Frederick, D. K., Sinden, F., *Modeling and Analysis of Dynamics Systems*, Wiley, New York, 1995.

Table 1 – Base Mass Properties

Parameter	Value	Units
m_B	50.5	gm
$SL_{G\to B}$	0.743	cm
$BL_{G\to B}$	0.0	cm
$WL_{G\to B}$	9.902	cm
I^B_{XX}	828.85	gm-cm^2
I^B_{YY}	872.55	gm-cm^2
I^B_{ZZ}	306.10	gm-cm^2
I^B_{XY}	0.0	gm-cm^2
I^B_{XZ}	-38.84	gm-cm^2
I^B_{YZ}	0.0	gm-cm^2

Table 2 – Rotor Mass Properties

Parameter	Value	Units
m_H	5.3	gm
$SL_{G\to H}$	0.0	cm
$BL_{G\to H}$	0.0	cm
$WL_{G\to H}$	0.0	cm
I_{XX}^{H}	92.15	gm-cm^2
I_{YY}^{H}	92.15	gm-cm^2
I_{ZZ}^{H}	184.30	gm-cm^2
I_{XY}^{H}	0.0	gm-cm^2
I_{XZ}^{H}	0.0	gm-cm^2
I_{YZ}^{H}	0.0	gm-cm^2

Table 3 – Initial Conditions

Parameter	Value	Units
x_0	0.0	cm
y_0	0.0	cm
z_0	-4.0	cm
ϕ_0	0.0	deg
θ_0	0.0	deg
ψ_0	0.0	deg
γ_0	0.0	deg
u_0	0.0	cm/s
v_0	0.0	cm/s
w_0	0.0	cm/s
p_0	0.0	rad/s
q_0	0.0	rad/s
r_0	0.0	rad/s
r_{H0}	0.0	rad/s

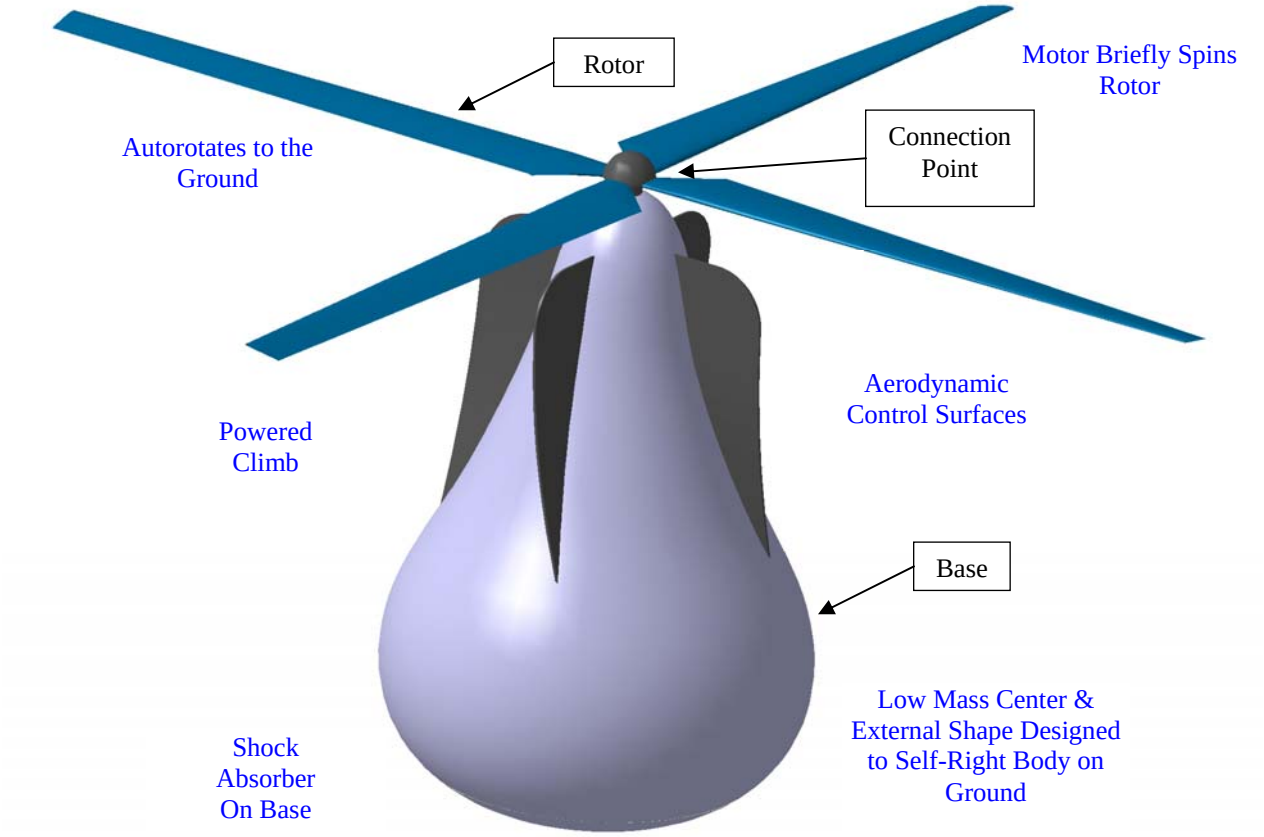

Figure 1 – Picture of a Hopping Rotochute and Highlights.

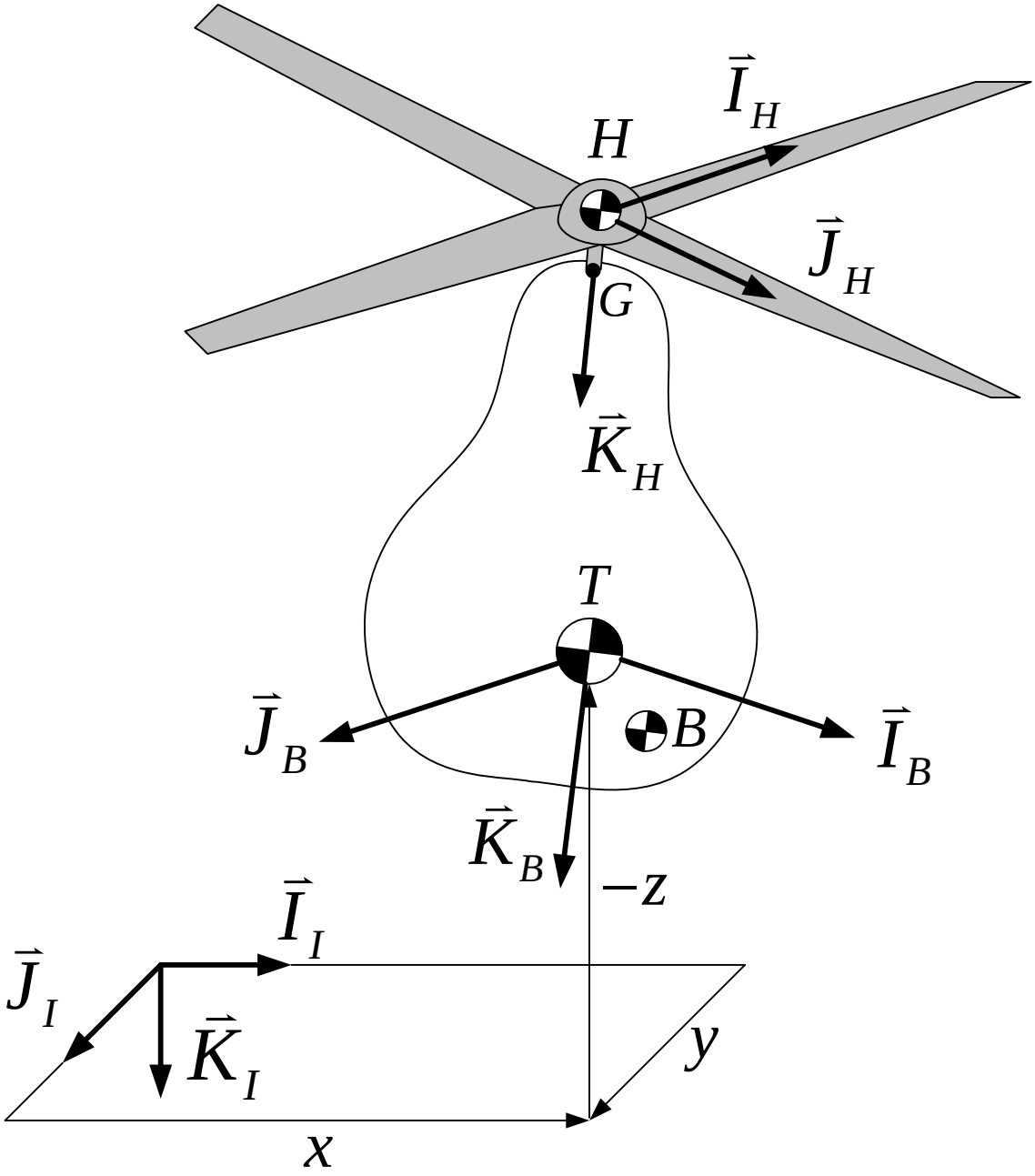

Figure 2 – Schematic of the Hopping Rotochute with Associated Reference Frames.

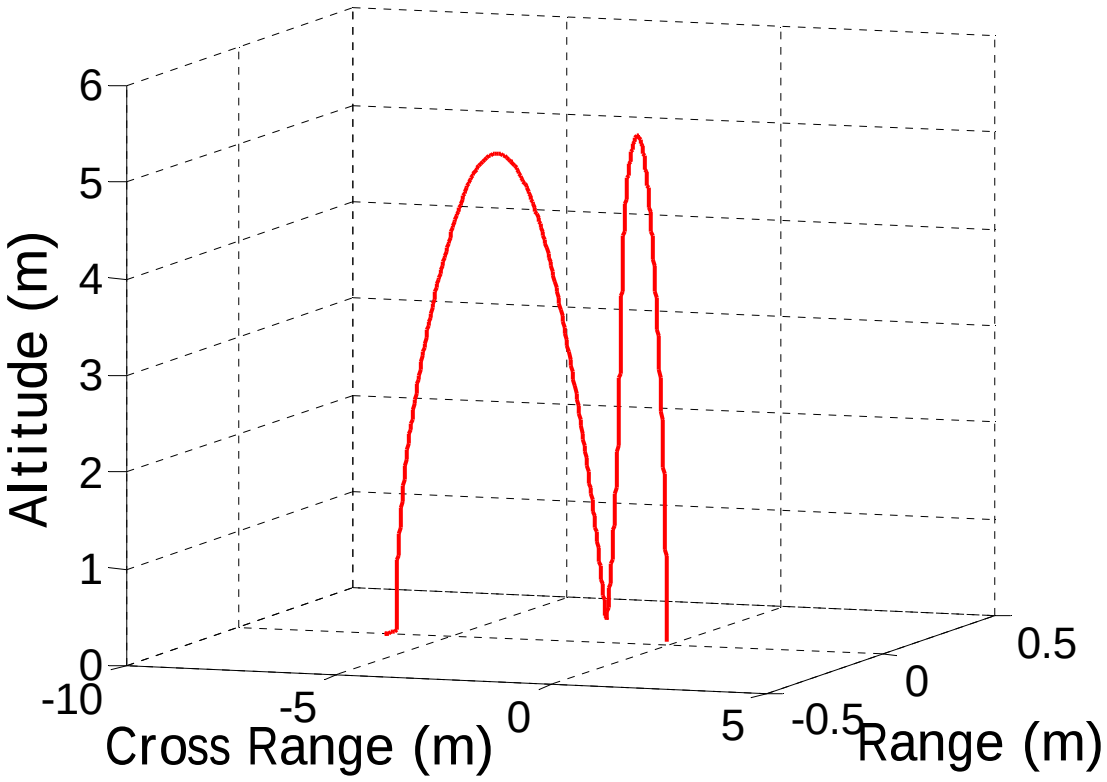

Figure 3 – Altitude versus Cross Range versus Range

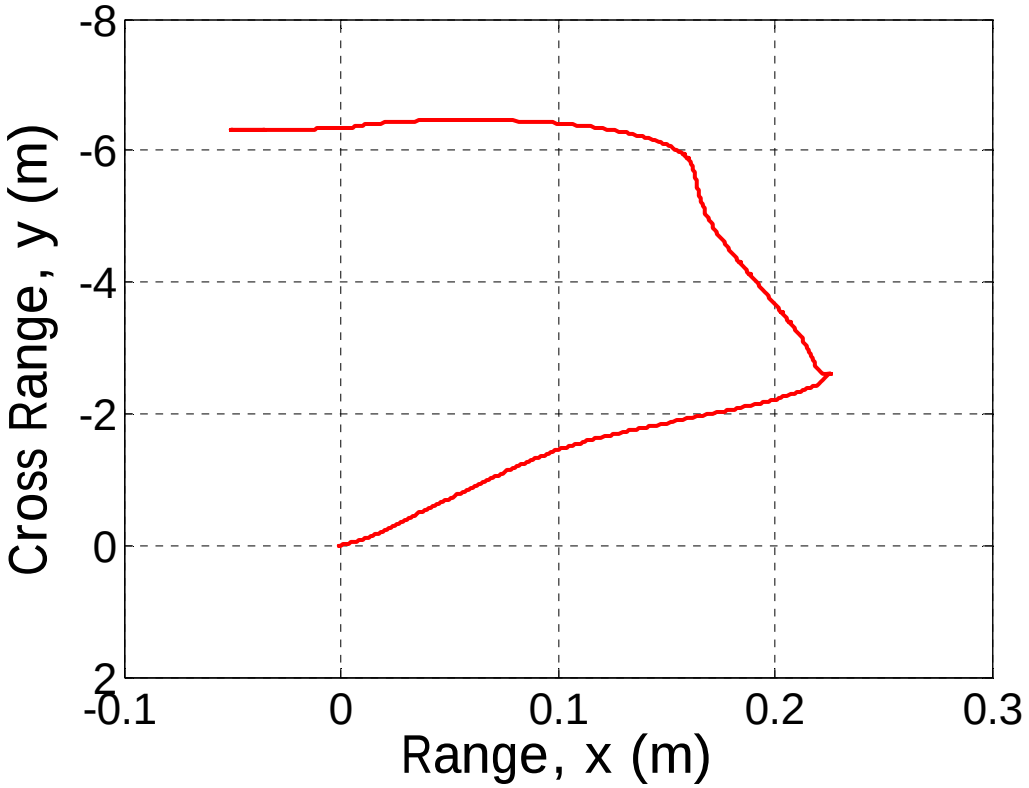

Figure 4 – Cross Range versus Range

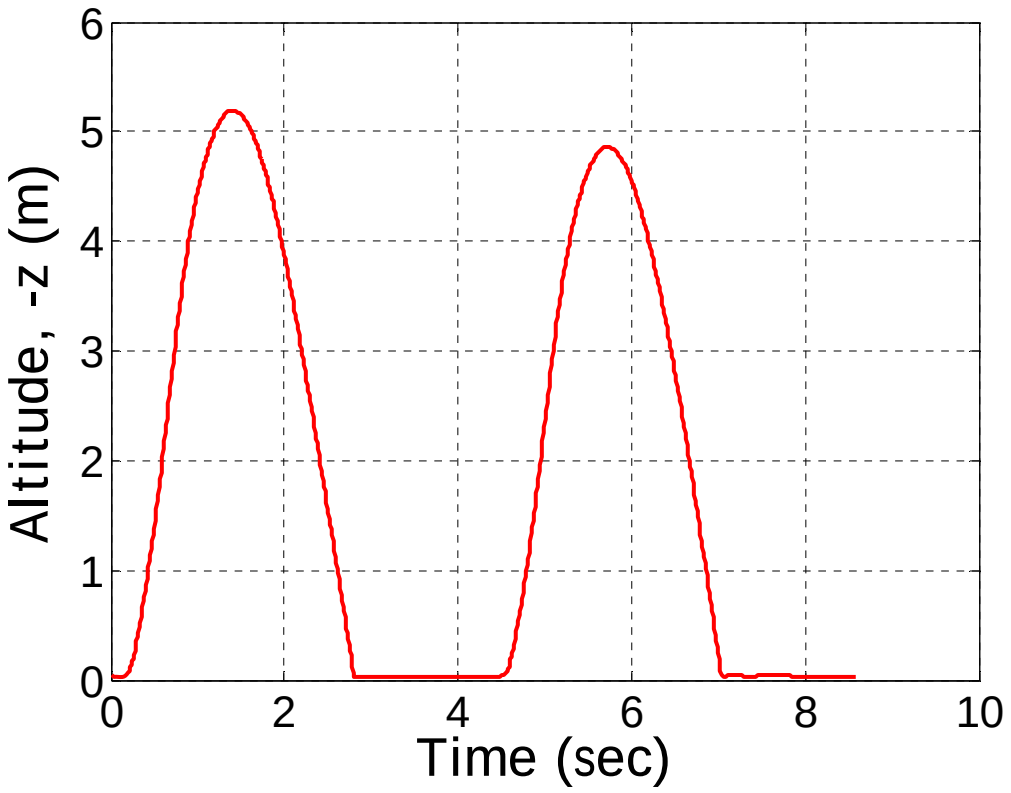

Figure 5 – Altitude versus Time

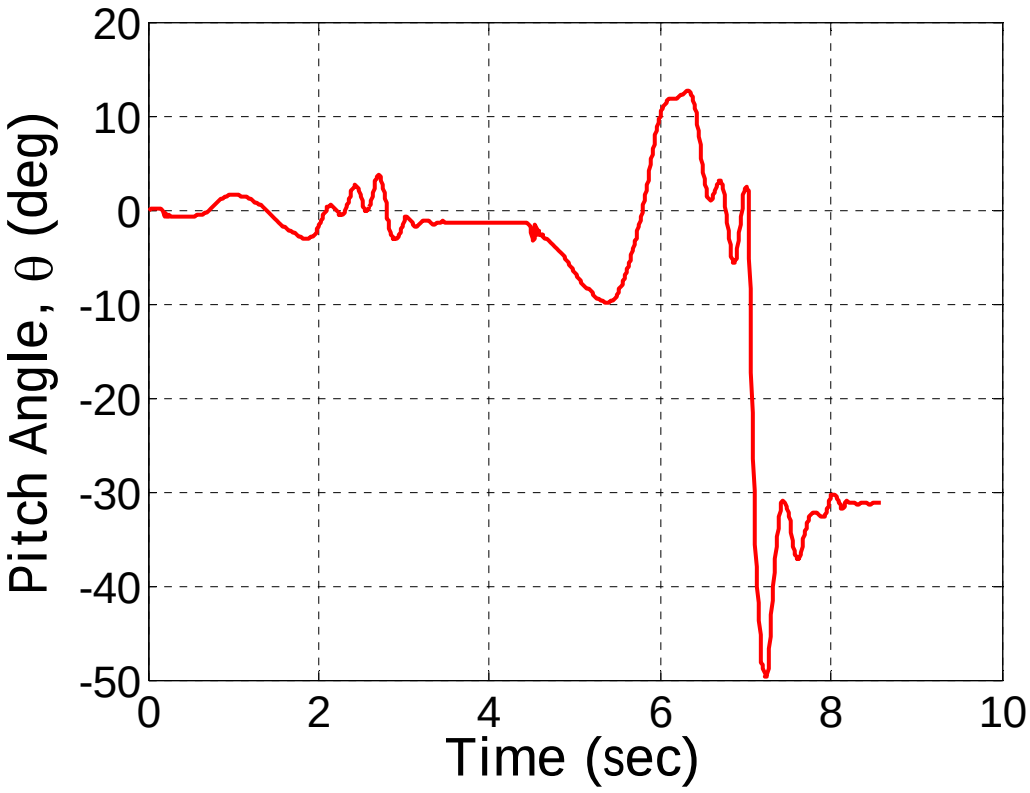

Figure 6 – Pitch Angle versus Time

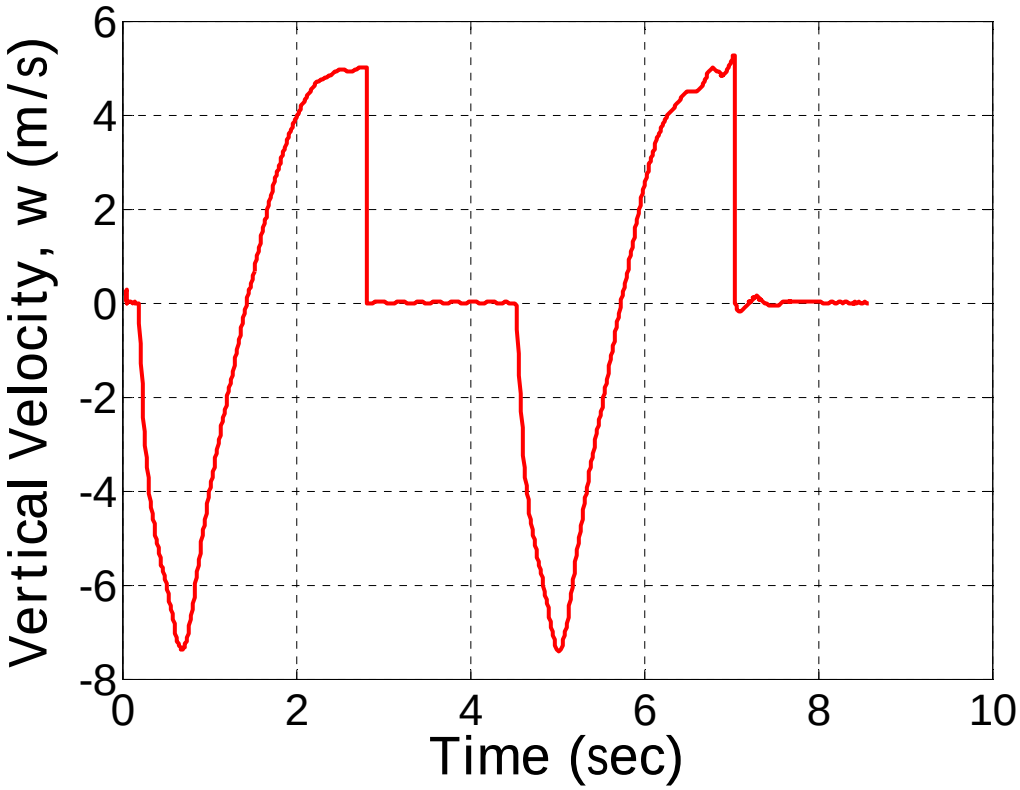

Figure 7 – Vertical Velocity versus Time

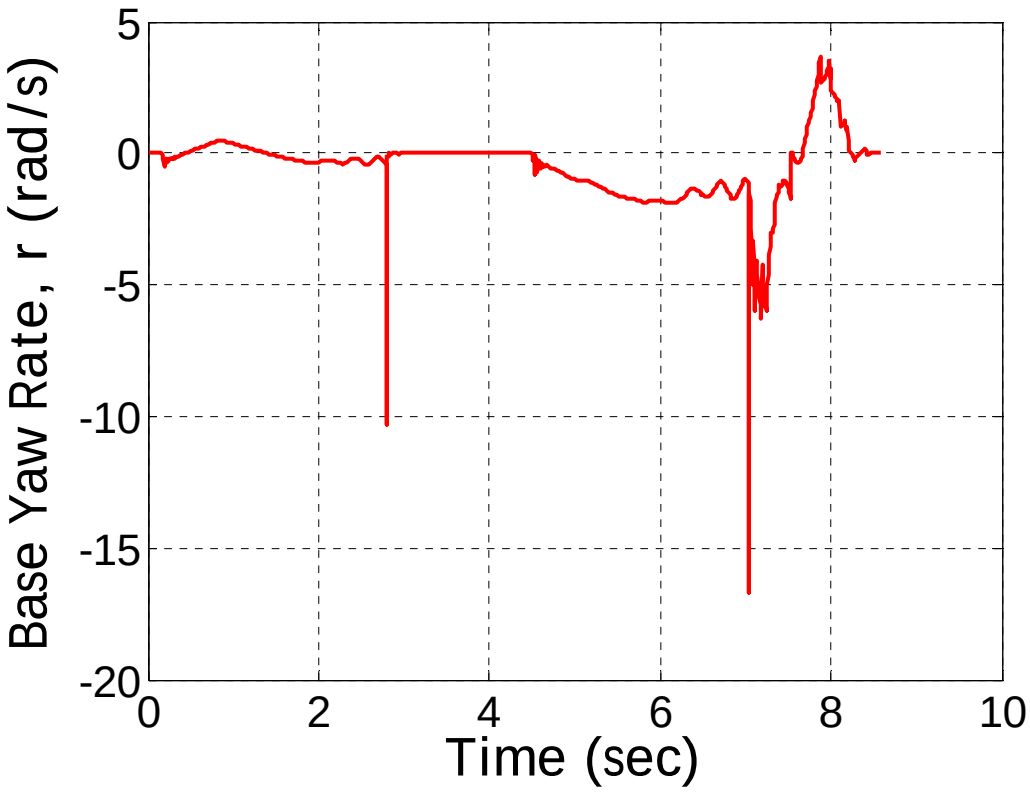

Figure 8 – Base Yaw Rate versus Time

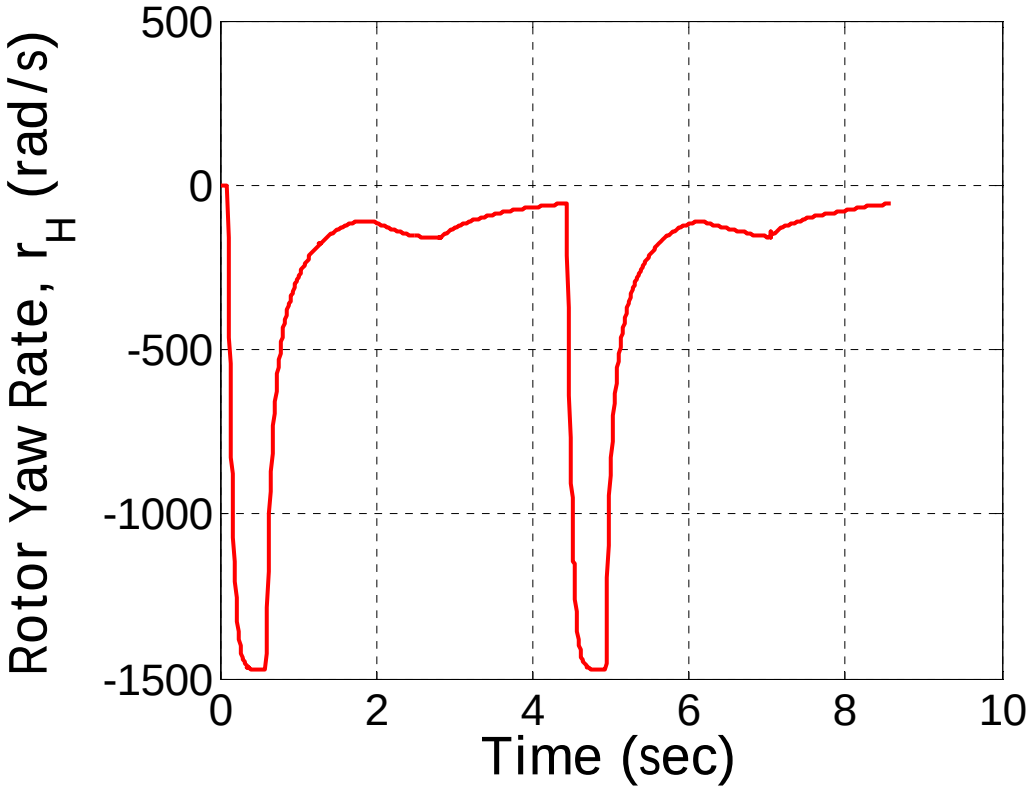

Figure 8 – Rotor Yaw Rate versus Time

Figure 9 – Prototype Hopping Rotochute

Figure 10 – Georgia Tech Indoor Flight Facility

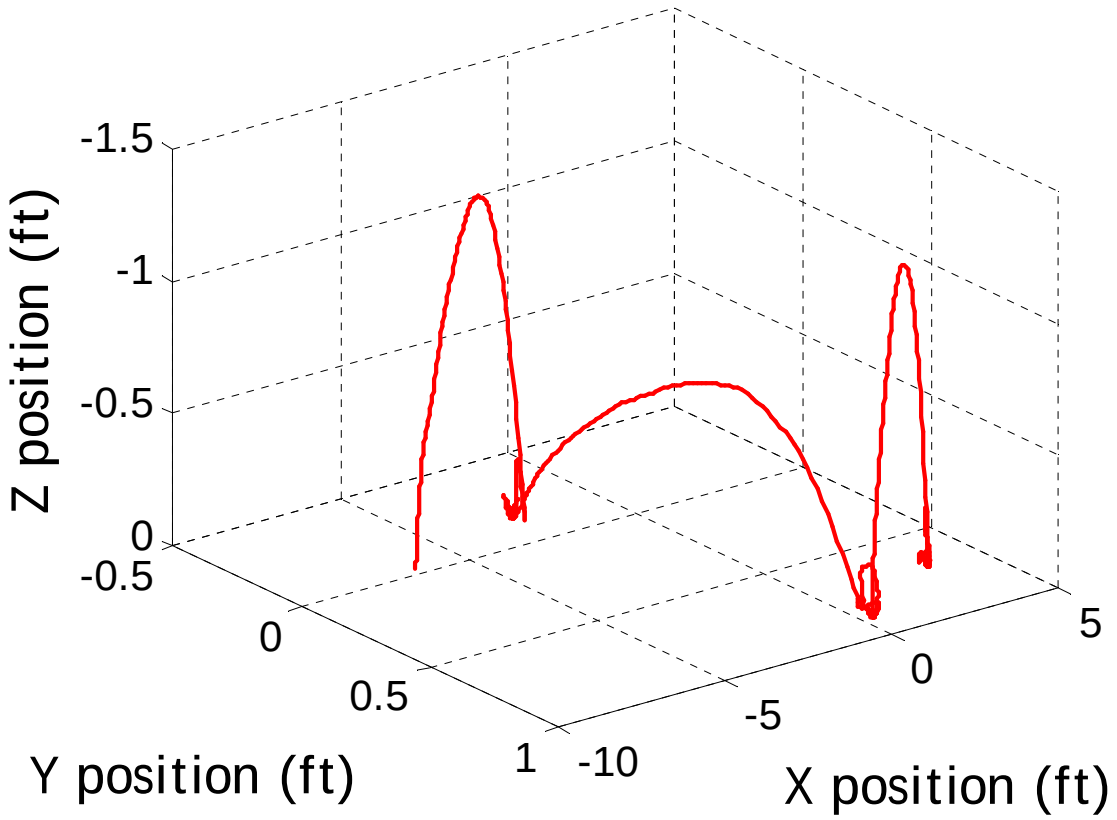

Figure 11 – Example Measurement Prototype Trajectory

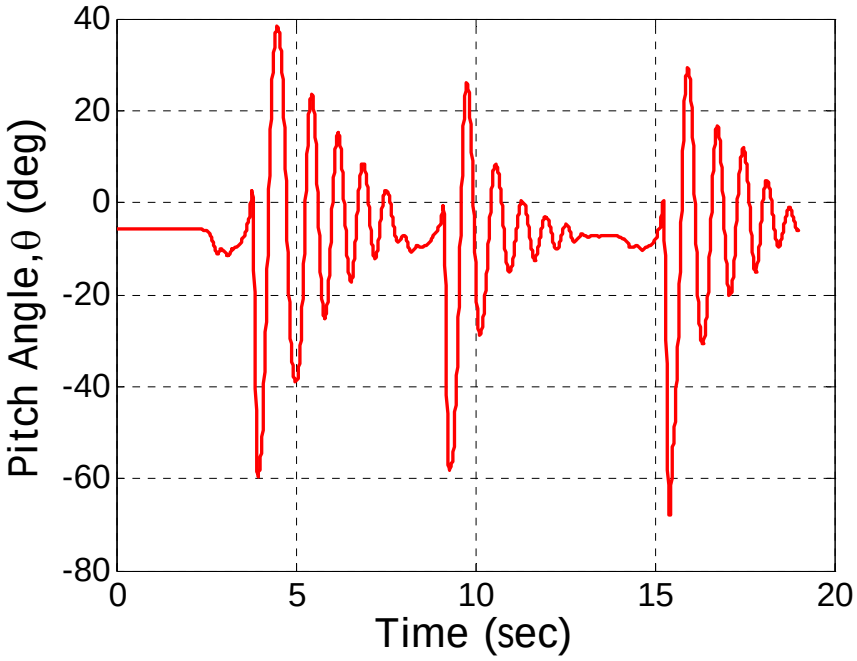

Figure 12 – Example Prototype Orientation